

Temperature Rise on Liner Surfaces of Fuel Cell Electric Vehicle Tanks during Fueling Process

Taichi Kuroki,* Cory Kreuzer, Daniel Leighton, Joshua Martin, Jeffrey Mohr, Michael Peters, Matthew Ruple, Onorato Shaun, and Steven Mathison

Herein, the temperature of the inner tank walls, or plastic liners, of composite pressure tanks in fuel cell electric vehicles during fueling using three-dimensional computational fluid dynamics (CFD) models is evaluated. The liner materials are limited to 85.0 °C to prevent thermal stress causing material failure that would result in a hydrogen leak. Therefore, the temperature of hydrogen gas must be limited to below 85.0 °C during the fueling process as dictated by the current fueling protocol. However, there are limited experimental or simulation data confirming that the temperature changes do not exceed the threshold. Herein, the liner temperatures with CFD tank models for two sizes of type IV tanks representative of the upper and lower system bounds that are close to the SAE J2601 fueling protocol (36.0 and 244.0 L) are evaluated. First, each model's reliability is validated with experimental data and then analyzed, and the data are used to evaluate the maximum hydrogen and liner temperatures under real-world fueling conditions. The evaluation shows that the maximum liner surface temperature of each tank model is at least 7 °C lower than that of the hydrogen. Additionally, there is at least 12 °C difference found between the upper limit and actual liner temperatures.

a polymer liner) that are fueled with pressurized hydrogen gas up to 70.0 MPa. The polymer liner materials (generally high-density polyethylene (HDPE) or similar chemistry) are designed as the primary hydrogen gas barrier and limit hydrogen permeation to within pressure vessel standards. The polymer materials are limited to a maximum temperature of 85.0 °C as the polymer structure can degrade or fracture due to thermal stresses building up, which could result in hydrogen leaks. Therefore, one method that industry adopted to mitigate heating during the refueling process was to precool the hydrogen gas to -40 °C, which helps prevent failure conditions from forming.

To promote the adoption of FCEVs by the public, a variety of studies have been conducted across the world.^[1-3] Elgowainy, Reddi, Lee, Rustagi, and Gupta^[4] conducted a techno-economic analysis of hydrogen precooling units on


1. Introduction

In the last several years, an emphasis has been placed on the development of fuel cell electric vehicles (FCEVs) along with fueling stations and infrastructure to support them. FCEVs operate using fuel cells that electrochemically react hydrogen gas with atmospheric oxygen to generate electricity that powers electric drivetrains. The vehicles utilize storage tanks (typically type IV) that are constructed of composite materials (carbon fiber with

the station side and proposed that a precooling unit consisting of a 13 kW refrigerator and a 1400 kg thermal mass would be optimal to reduce the operational costs of fueling stations. Kim et al.^[5] conducted a risk assessment analysis for hydrogen storage tanks and proposed a safe design to avoid hydrogen leaks. Thanks to these studies, as well as new technologies, such as safety designs, hydrogen production and transportation, and increased fuel cell efficiency, FCEVs have the potential to be readily adopted in the mainstream transportation sector.

The technology to fill FCEV tanks safely and quickly with hydrogen has been built upon studies that evaluate the hydrogen temperature rise in FCEV tanks during fast fillings in experiments and numerical simulations.^[6-14] Dicken et al. measured the hydrogen temperature at 36 locations within a type III FCEV tank, while the tank was filled up to 35.0 MPa under different initial hydrogen pressures; they reported that the thermal fields in the vehicle tank were almost uniform during the fueling process regardless of the variation of the initial gas pressures.^[15] Kaifeng et al. performed 3D computational fluid dynamics (CFD) simulations with type III FCEV tanks. The authors initially validated the reliability of the tank models with experimental data and then evaluated the flow pattern within the tank models and the effect of heat transfer from the hydrogen to the tank walls.^[16] With the development of hydrogen fueling technology, a hydrogen fueling protocol was established by SAE J2601.^[17]

T. Kuroki, C. Kreuzer, D. Leighton, J. Martin, J. Mohr, M. Peters, M. Ruple, O. Shaun, S. Mathison
Energy Conversion and Storage Systems Center
National Renewable Energy Laboratory
Golden, CO 80401, USA
E-mail: taichi.kuroki@nrel.gov

 The ORCID identification number(s) for the author(s) of this article can be found under <https://doi.org/10.1002/ente.202300239>.

© 2023 The Authors. Energy Technology published by Wiley-VCH GmbH. This is an open access article under the terms of the Creative Commons Attribution-NonCommercial-NoDerivs License, which permits use and distribution in any medium, provided the original work is properly cited, the use is non-commercial and no modifications or adaptations are made.

DOI: 10.1002/ente.202300239

Currently, the protocol dictates that the temperature of hydrogen in FCEV tanks during the fueling process shall be below 85.0 °C, which is attributed to the maximum exposure temperature of the liner material of type IV tanks. The protocol assumes that both hydrogen gas and liner temperatures increase at the same rate during the fueling process. Nevertheless, the assumption has not yet been validated extensively with experimental or simulation data, and the relationship between the maximum hydrogen temperature and liner material temperature has not been quantitatively revealed. This is because previous studies (including those cited in ref. [6–16]) focus on the hydrogen temperature in FCEV tanks during the fueling process and do not evaluate the temperature of the liners. From a safety perspective, it is vital to understand the temperature rise of the liner material in relation to hydrogen gas temperature during the fueling process to prevent material failure and a potential hydrogen leak.

To evaluate the aforementioned points, this study utilizes CFD software, ANSYS FLUENT, because Kaifeng et al.^[16] and other researchers^[18–21] prove that 3D CFD simulations are a sufficiently effective approach to comprehend the thermal and flow fields inside FCEV tanks as well as the temperature distributions within the tank walls. This study leverages a high-performance computing system at the National Renewable Energy Laboratory (NREL) to run 3D CFD simulations. CFD makes it possible to evaluate temperatures at any location in the control domain; thus, details of both the hydrogen and liner thermal fields can be investigated. This study initially builds 36.0 and 244.0 L tank models that correspond approximately to the minimum and maximum onboard storage system sizes defined in SAE J2601.^[17] With these tank models, this study simulates the thermal and flow fields of hydrogen inside each tank model under the same

conditions as in fueling experiments conducted with 36.0 and 244.0 L test tanks. This allows an evaluation of the temperature rise of both hydrogen and liner with real-world fueling conditions while enabling this study to validate the reliability of the tank models. Through these efforts, this study quantitatively evaluates how quickly the change in the liner temperatures follow that of the incoming hydrogen gas's temperature fluctuations and determines the differential temperature between the hydrogen and liner material. The temperature data of the hydrogen and liner material should make it possible to assess how safe the current SAE J2601 fueling protocol is, as well as suggesting possible improvements to the protocol.

2. Simulation Models, Methodology, and Conditions

This study built two CFD FCEV tank models shown in **Figure 1a, b**: 36.0 and 244.0 L type IV tank models. Each of the tank models consist of an injector with an internal diameter of 5.0 mm and a length of 100.0 mm, a plastic liner, and a carbon fiber-reinforced plastic (CFRP). The thermodynamic properties of the liner and CFRP materials are close to the values shown in **Table 1** that are set by the SAE J2601 standard.^[17] Both tank models are assumed to be horizontally oriented, as the test tanks described in the next section were horizontally oriented. The geometries of the solid and fluid regions were generated with hexahedral meshes, and the number of meshes for the 36.0 and 244.0 L tanks is approximately 240 000 and 780 000, respectively.

In solving the thermal and fluid fields inside each tank model, the unsteady form of the continuity, Reynolds-averaged Navier–

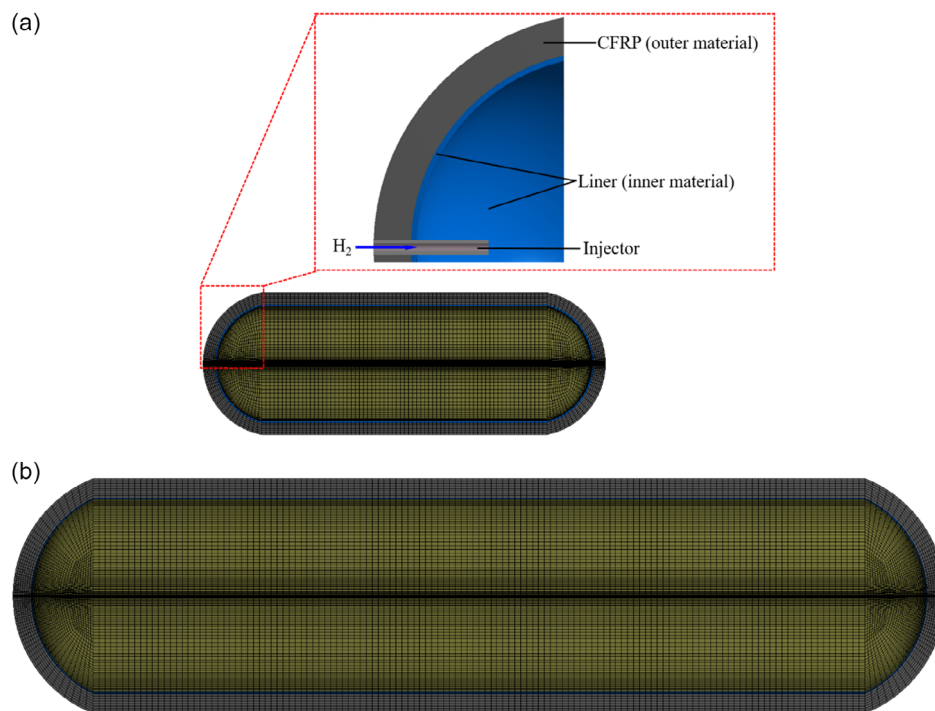


Figure 1. FCEV tank models a) 36.0 L and b) 244.0 L.

Table 1. Thermophysical properties for liner and CFRP materials.

	Thermal conductivity [W m ⁻¹ K ⁻¹]	Heat capacity [J kg ⁻¹ K ⁻¹]	Density [kg m ³]
Liner	0.5	2100.0	945.0
CFRP	0.5	1120.0	1494.0

Stoke, and energy equations for flows involving heat transfer and compressibility were solved. Those conservation equations are given by

$$\frac{\partial \rho}{\partial t} + \frac{\partial}{\partial x_i} (\rho u_i) = 0 \quad (1)$$

$$\frac{\partial}{\partial t} (\rho u_i) + \frac{\partial}{\partial x_i} (\rho u_i u_i) = -\frac{\partial P_i}{\partial x_i} + \frac{\partial}{\partial x_j} \left[\mu \left(\frac{\partial u_i}{\partial x_j} + \frac{\partial u_j}{\partial x_i} - \frac{2}{3} \delta_{ij} \right) \right] - \frac{\partial}{\partial x_j} (\overline{\rho u_i' u_j'}) + \rho \vec{g} \quad (2)$$

$$\frac{\partial}{\partial t} (\rho E) + \frac{\partial}{\partial x_i} (u_i (\rho E + P)) = \frac{\partial}{\partial x_j} \left[k_{\text{eff}} \frac{\partial T}{\partial x_j} + u_i (\tau_{ij})_{\text{eff}} \right] \quad (3)$$

where ρ is the density, u is the velocity, t is the time, P is the static pressure, g is the gravitational acceleration, μ is the dynamic viscosity, δ_{ij} is the Kronecker delta, E is the total energy, h is the specific enthalpy, and T is the temperature. The total energy is expressed as

$$E = h - \frac{P}{\rho} + \frac{1}{2} u_i^2 \quad (4)$$

The k_{eff} is the effective thermal conductivity given by

$$k_{\text{eff}} = k + \frac{C_p \mu_t}{Pr_t} \quad (5)$$

where k is the thermal conductivity, C_p is the specific heat at constant pressure, μ_t is the turbulent viscosity, and Pr_t is the turbulent Prandtl number. The $(\tau_{ij})_{\text{eff}}$ is the deviatoric stress tensor defined as

$$(\tau_{ij})_{\text{eff}} = \mu_{\text{eff}} \left(\frac{\partial u_i}{\partial x_j} + \frac{\partial u_j}{\partial x_i} \right) - \frac{2}{3} \mu_{\text{eff}} \frac{\partial u_k}{\partial x_k} \delta_{ij} \quad (6)$$

where

$$\mu_{\text{eff}} = \mu + \mu_t \quad (7)$$

For the turbulence model, the realizable k - ϵ model was applied. The transport equations for turbulent kinetic energy, k , and dissipation rate, ϵ , are shown as follows

$$\frac{\partial (\rho k)}{\partial t} + \frac{\partial (\rho k u_j)}{\partial x_j} = \frac{\partial}{\partial x_j} \left[\left(\mu + \frac{\mu_t}{\sigma_k} \right) \frac{\partial k}{\partial x_j} \right] + G_k + G_b - \rho \epsilon - Y_M \quad (8)$$

$$\frac{\partial (\rho \epsilon)}{\partial t} + \frac{\partial (\rho \epsilon u_j)}{\partial x_j} = \frac{\partial}{\partial x_j} \left[\left(\mu + \frac{\mu_t}{\sigma_\epsilon} \right) \frac{\partial \epsilon}{\partial x_j} \right] + \rho_1 C_1 S \epsilon - \rho C_2 \frac{\epsilon^2}{k + \sqrt{v \epsilon}} + C_{1\epsilon} \frac{\epsilon}{k} C_{3\epsilon} G_b \quad (9)$$

where

$$\text{if } \frac{\eta}{\eta + 5} \leq 0.43, \quad C_1 = 0.43 \quad (10)$$

$$\text{if } \frac{\eta}{\eta + 5} > 0.43, \quad C_1 = \frac{\eta}{\eta + 5} \quad (11)$$

$$\eta = S \frac{k}{\epsilon} \quad (12)$$

$$S = \sqrt{2 S_{ij} S_{ij}} \quad (13)$$

In Equation (9)–(13), η is the effectiveness factor, S is the magnitude of vorticity, S_{ij} is the mean strain rate, C_2 , $C_{1\epsilon}$, and $C_{3\epsilon}$ are constants, and σ_k and σ_ϵ are the turbulent Prandtl numbers for k and ϵ that are constants. Those constants C_2 , $C_{1\epsilon}$, $C_{3\epsilon}$, σ_k , and σ_ϵ are 1.44, 1.9, 1.0, 1.0, and 1.2.^[22] G_k represents the production of turbulence kinetic energy given by

$$G_k = -\rho \overline{u_i' u_j'} \frac{\partial u_j}{\partial x_i} \quad (14)$$

G_b represents the generation of turbulence due to buoyancy and is expressed by

$$G_b = \beta g \frac{\mu_t}{Pr_t} \frac{\partial T}{\partial x_i} \quad (15)$$

where β is the coefficient of thermal expansion obtained by

$$\beta = -\frac{1}{\rho} \left(\frac{\partial \rho}{\partial T} \right) \quad (16)$$

Y_M represents the contribution of the fluctuating dilation in compressible turbulence to the overall dissipation rate and is given by

$$Y_M = 2 \rho \epsilon M_t^2 \quad (17)$$

where M_t is the turbulent Mach number defined as

$$M_t = \sqrt{\frac{k}{a^2}} \quad (18)$$

In Equation (18), a is the speed of sound.

The conservation equations and turbulence model were discretized and solved with a time step, δt , of 1.0×10^{-3} s in the commercial CFD software ANSYS FLUENT version 19.2. For the pressure–velocity coupling, the semi-implicit method for pressure-linked equations (SIMPLE) algorithm was applied. For the spatial discretization scheme, the second-order upwind scheme was set.^[22] In terms of the pressure interpolation, pressure staggering option (PRESTO) scheme was utilized.^[22]

While the hydrogen is being fueled into each tank model, the hydrogen temperature and pressure change significantly. With

the change in the temperature and pressure, thermophysical properties, such as the thermal conductivity, viscosity, and specific heats at constant volume and pressure, change considerably. Precision in the thermophysical properties is crucial to accurately simulate the thermal and flow fields of hydrogen in the tank models during the fueling process; therefore, this study leveraged the National Institute of Standards and Technology (NIST) real gas model, or REFPROP, in the CFD simulations.^[23] By coupling the real gas model for hydrogen to the conservation equations and turbulence model shown in Equation (1)–(18), the thermal and flow fields inside each tank model were simulated. When the density residual of each iteration is reduced to 1.0×10^{-3} , this study defines the iteration as convergent.

3. Hydrogen Fueling Experiments

This study leveraged experimental fueling data collected with 36.0 and 244.0 L type IV tanks, which are made of a plastic liner and CFRP, to validate the CFD tank models developed in Section 2. A summary of each fueling experiment is shown in Table 2. This section describes each of the experimental setups, experimental conditions, and collected data.

3.1. Hydrogen Fueling Experiment with 36.0 L Tank

The experimental data with a 36.0 L tank were collected at NREL's research fueling station at the Hydrogen Infrastructure Testing and Research Facility (HITRF). The experimental setup focused on the area downstream of the dispenser is shown in Figure 2. This study assumed the onboard storage system size to be 108.0 L by using three 36.0 L tanks as shown in

Figure 2. Figure 2 also shows that the temperature of hydrogen delivered from the dispenser to the 36.0 L tanks was measured immediately after the fueling receptacle and at a central position in one of the 36.0 L tanks. The experimental conditions when the hydrogen fueling experiment was conducted are shown in Table 2. The temperature and pressure of hydrogen flowing inside the supply line are shown in Figure 3. The black line represents the temperature at the receptacle exit, and the red line indicates the pressure at one of the 36.0 L tank inlets. In the experiment, the initial pressure at the tank inlet was 6.3 MPa before the fueling experiment and increased up to 73.0 MPa in 186.0 s as shown in Table 2. The average pressure ramp rate (APRR) calculated from the initial and final pressures and the fueling was $19.1 \text{ MPa min}^{-1}$ even though the APRR set to the dispenser was $19.7 \text{ MPa min}^{-1}$ (Table 2 shows both the set and actual APRRs). The hydrogen temperature at the receptacle was initially equivalent to the ambient. At the start of the fueling process, the hydrogen temperature at the receptacle cooled down to around $-35 \text{ }^\circ\text{C}$ because hydrogen was chilled by a heat exchanger installed upstream of the dispenser. The hydrogen temperature in the test tank increased up to $65.7 \text{ }^\circ\text{C}$.

The temperature measured inside the 36.0 L tank was used to validate the reliability of the 36.0 L tank model. To compare the experimental data with the CFD simulation results, the experimental data shown in Figure 3 were used to define the boundary conditions of the tank model at the inlet. The initial hydrogen and tank wall temperatures were set to the ambient temperature in Table 2, and the initial hydrogen pressure was set to the value found in Table 2. After those boundary and initial conditions are set to the tank model, the thermal and flow fields inside the tank model were simulated.

Table 2. Summary of fueling experiments used to validate CFD tank models (ref. [28]).

Experiment facility	Vehicle tank storage system [L]	$T_{\text{initial}} (T_{\text{amb}})$ [$^\circ\text{C}$]	P_{initial} [MPa]	Set APRR (actual APRR) [MPa min^{-1}]	Fueling time [s]	P_{initial} [MPa]	T_{final} [$^\circ\text{C}$]	
Exp. 1	NREL	108.0 (3 × 36.0)	23.0	6.3	19.8 (19.1)	186.0	73.0	65.7
Exp. 2	Powertech (ref. [28])	244.0	19.5	2.1	19.4 (14.5)	310.0	71.6	76.5
Exp. 3			50.0	5.2	7.6 (7.6)	536.0	80.3	76.2

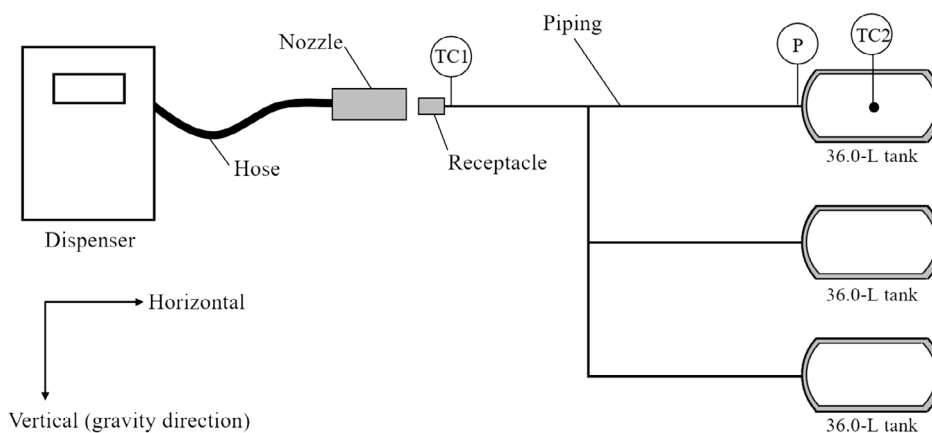


Figure 2. Schematic diagram of experimental setup with 108 L storage system consisting of three 36.0 L tanks.

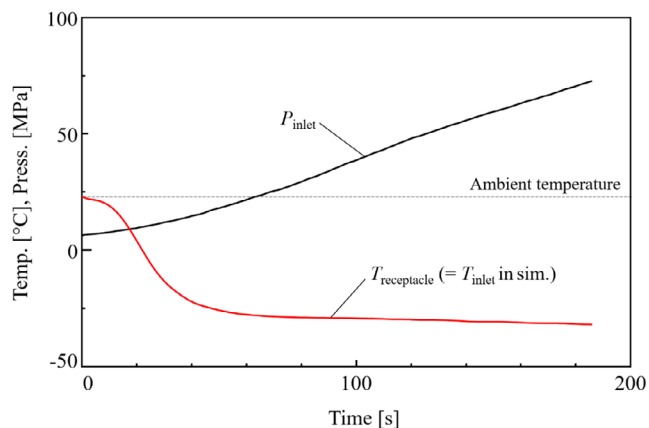


Figure 3. Temperature measured at 36.0 L tank inlet and pressure measured at receptacle; the temperature and pressure profiles were used to perform a CFD simulation in Section 4.1. Fueling conditions: an ambient temperature of 23.0 °C, an initial gas pressure of 6.3 MPa, and an APRR of 19.1 MPa min⁻¹.

3.2. Hydrogen Fueling Experiments with 244.0 L Tank

For the validation of the 244.0 L tank model, the study leveraged experimental data that were collected at Powertech Lab’s hydrogen fueling test facility, for the establishment of the SAE J2601 fueling protocol.^[17] **Figure 4** shows part of the experimental setup where this study focused on the components downstream of the dispensers, which describes the temperature and pressure measurement positions for the experiments with the 244.0 L test tank. In each experiment, the temperature and pressure of hydrogen delivered to the test tank were measured at the inlet of the test tank. With respect to the temperature measurement inside the test tank, as shown in **Figure 4**, the hydrogen temperature was measured with a single thermocouple mounted around the tank wall directly opposite the tank inlet, TC2, and the temperature on the liner surface was also measured around the inner back-tank wall, TC3. These thermocouple positions were chosen because the tank size was larger, and therefore the hydrogen’s temperature distribution inside the tank was less uniform. The nonuniformity of the temperature distribution causes a significantly higher than average gas temperature at a local position

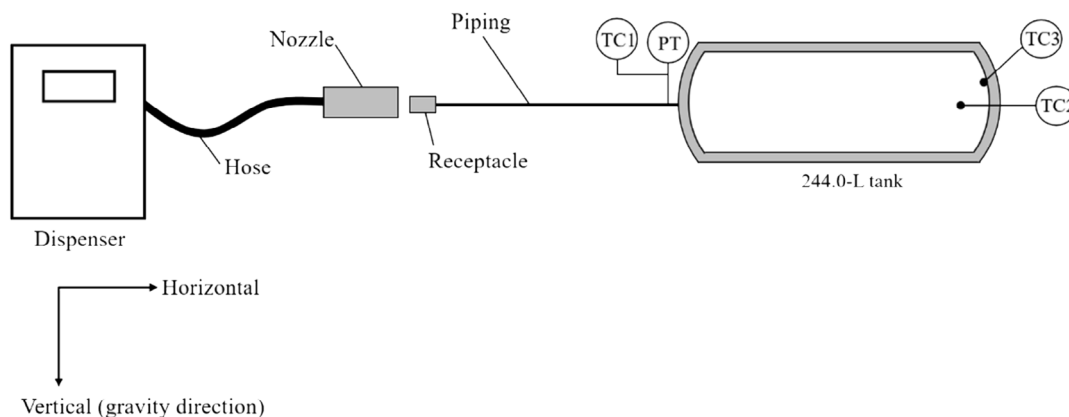


Figure 4. Schematic diagram of experimental setup with 244.0 L tank.

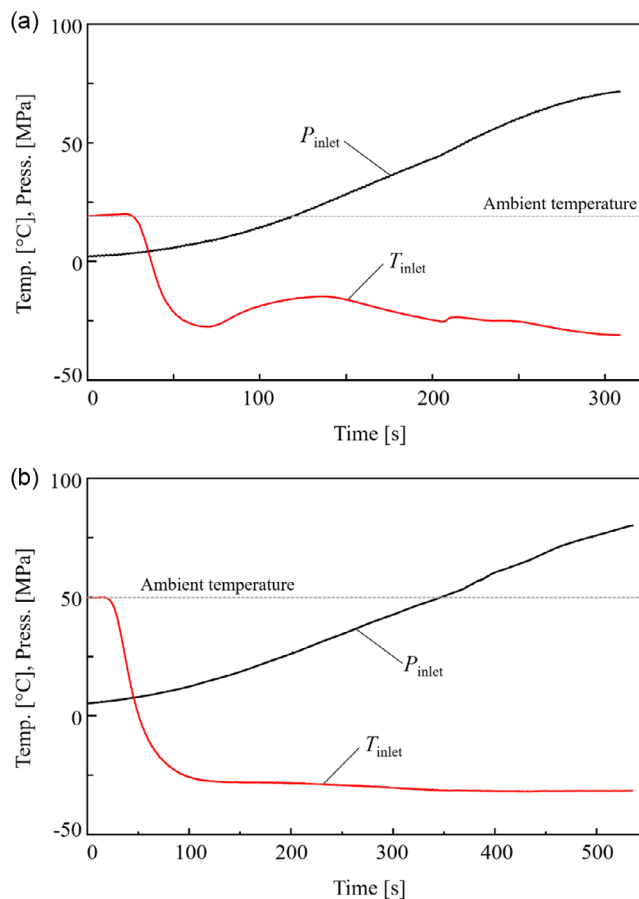


Figure 5. Temperature and pressure measured at 244.0 L tank inlet. a) Fast-fill experiment: an ambient temperature of 19.5 °C, an initial gas pressure of 2.1 MPa, and an APRR of 14.5 MPa min⁻¹. b) Slow-fill experiment: an ambient temperature of 50.0 °C, an initial gas pressure of 5.2 MPa, and an APRR of 7.6 MPa min⁻¹. These data are used to perform a CFD simulation in Section 4.2.

inside the tank. For this reason, two types of fueling data with the 244.0 L test tank (fast- and slow-fills) were used to evaluate which fill scenarios most strongly influenced the maximum surface temperature of the liner. **Figure 5** shows the hydrogen

temperature and pressure measured at the tank inlet, and those profiles were used as the boundary conditions of the tank model at the inlet. The black line represents pressure, and the red line represents temperature.

For the fast-fill experiment, the hydrogen pressure was initially 2.1 MPa and increased up to 71.6 MPa at a rate of 14.5 MPa min⁻¹, and the total fueling time was 310.0 s. For the slow-fill experiment, the initial hydrogen pressure in the test tank was 5.0 MPa and reached 80.3 MPa at the end of the fill in 536.0 s, and the calculated APRR was 7.6 MPa min⁻¹. In each experiment, the hydrogen was precooled by a heat exchanger upstream of the dispenser to keep the hydrogen temperature from exceeding 85.0 °C. Figure 5a shows that the hydrogen temperature at the tank inlet was cooled to a minimum of -31.0 °C in the fast-fill experiment, and Figure 5b shows that the tank inlet hydrogen temperature was reduced to a minimum of -32.0 °C in the slow-fill experiment. Due to the precooled hydrogen, in the fast-fill experiment, the ending hydrogen temperature was only 76.5 °C, and the ending gas temperature in the slow-fill experiment with a high ambient temperature was only 76.2 °C. The temperature rise in each experiment is detailed in Section 4.2. Each temperature and pressure profile measured at the test tank inlet was used to perform the CFD simulations by setting those profiles to the inlet of the tank model as the supply (boundary) conditions. In each simulation, the initial hydrogen and tank wall temperatures were set to the ambient temperature shown in Table 2, and the initial hydrogen pressure was set to the value found in Table 2. After those boundary and initial conditions were set to the tank model, the thermal and flow fields inside the tank model were simulated.

4. Validation of CFD Tank Models

4.1. Comparison of Simulation and Experimental Data with 108 L Storage System Consisting of Three 36.0 L Tanks

The simulation result with the 36.0 L tank model was compared with the corresponding experimental data and is shown in Figure 6. The temperatures simulated and measured at the center position of the test and modeled tanks are shown with the solid black line representing the experimental data, and the dashed red line representing the simulation result.

As Figure 6 shows, the initial gas temperature measured in the test tank was around 10 °C higher than the ambient. The disparity was caused during a start-up period right before the fueling experiment, as part of the leak checking process,^[14,17] where a small amount of hydrogen was supplied to the 108.0 L storage system in a short duration pulse to confirm whether the nozzle and receptacle are completely connected. As the small amount of hydrogen expanded inside the tank, the hydrogen temperature in the test tank rapidly increased, recognized as the Joule–Thomson effect. However, after the fueling process started, the difference in the initial temperatures in the experiment and simulation instantaneously disappeared. This demonstrates that the amount of hydrogen supplied during the connection pulse was much smaller in comparison with the amount delivered at the early stage of the fueling process.

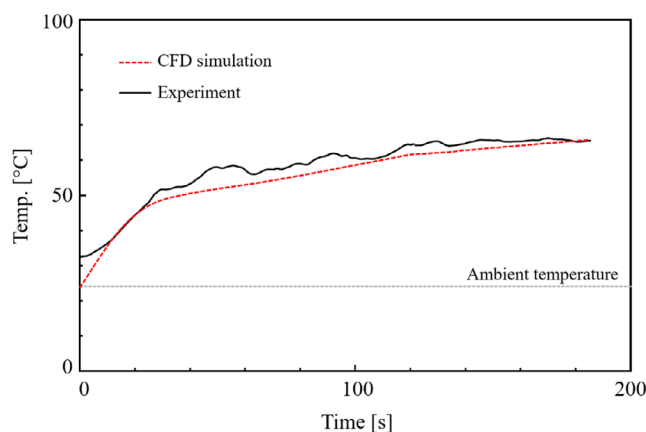


Figure 6. Validation of 36.0 L CFD tank model against measured hydrogen temperature under fast-fill condition. The comparison was conducted at an ambient temperature of 23.0 °C, an initial gas pressure of 6.3 MPa, and an APRR of 19.1 MPa min⁻¹.

The dynamic behaviors of both simulated and measured temperatures were consistent throughout the fueling process, and the measured temperature was always just a few degrees Kelvin higher than the simulation data. This is likely due to an assumption described in Section 3 in which this study uses the temperature measured at the receptacle as the tank inlet temperature for the simulation. The true hydrogen temperature at the inlet of the experimental tank was likely higher than the value measured at the receptacle due to the thermal mass of the piping and fittings along the distribution piping from the receptacle to the tank inlet, as well as heat gain from convection with the ambient air along this section. This assumption may have resulted in the simulated gas temperature being higher than that of the measured data. Despite this variance, the comparison shows that the 36.0 L tank model was able to simulate the measured experimental temperature with good accuracy. The maximum discrepancy was 6.3 °C, which occurred at around 50 s when the measured temperature fluctuated unsteadily. This study deduces that the jet from the injector may have caused the oscillation of the temperature measurement because the distance between the injector outlet and temperature sensor is approximately 0.35 m, which is not large. If the temperature sensor did not include the jet's influence, the simulation and experimental data would be closer. In this scenario, even though this study compared the CFD and experimental data only at a single location, the 36.0 L tank model is reliable.

4.2. Comparison of Simulation and Experimental Data with 244.0 L Tank

Figure 7 and 8 show the experimental and simulation data obtained with the 244.0 L test and modeled tanks. Figure 7 shows the comparison of the fast-fill data, and Figure 8 shows the comparison of the slow-fill data. The temperature evaluation positions in the experiment and CFD simulation correspond to the mounting positions of the thermocouples in Figure 4. Each solid line represents the experimental data, and the dashed line represents the simulation result.

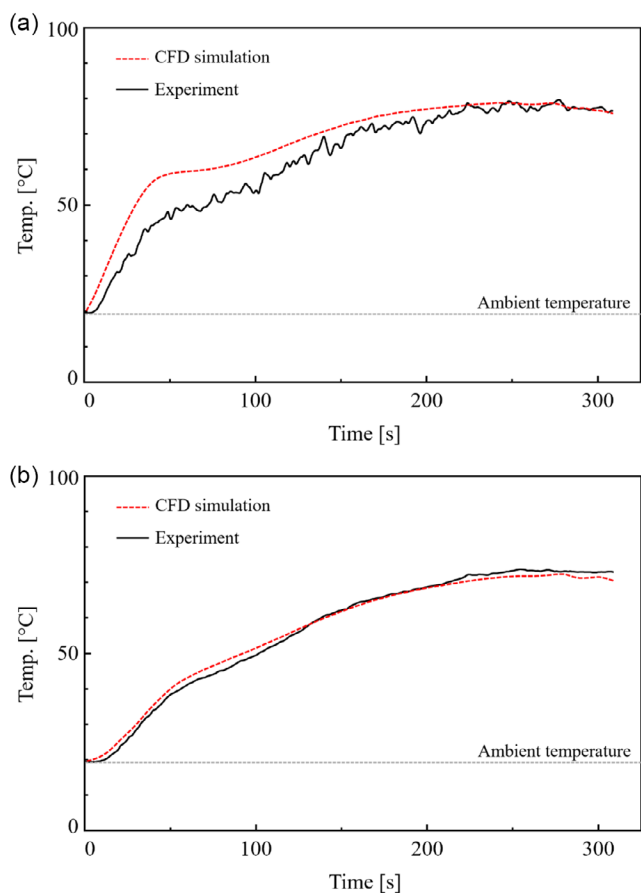


Figure 7. Validation of 244.0 L CFD tank model against corresponding experimental fueling data for the fast-fill condition. a) Hydrogen temperature, TC2. b) Liner surface temperature, TC3. The comparison was conducted under the following fueling conditions: an ambient temperature of 19.5 °C, an initial gas pressure of 2.1 MPa, and an APRR of 14.5 MPa min⁻¹.

For the comparison of the fast-fill data, the dynamic behavior of the simulated hydrogen temperature was consistent with the experimental data throughout the fueling process. In this experiment, the connection pulse and leak checks were not conducted before the fueling process started, and therefore, the hydrogen temperature in the test tank started from the ambient. The maximum discrepancy between the measured and simulated temperatures was around 10 °C, which occurred at the early stage of the fill. This discrepancy could be due to a large time constant of the thermocouple, TC2. As evidence to support the rationale, the difference in the measured and simulated temperatures was only 1.0 °C at the end of the fill. When the fueling process approaches the end of the fill, the temperature change over time becomes small. Therefore, the uncertainty associated with the thermocouple's time constant is significantly reduced at the end of the fill. Additionally, the jet from the injector may have affected the temperature measurement. The thermocouple, TC2, is located where the jet from the injector directly hit when the jet reaches the back tank wall. The influence of the jet from an FCEV tank injector is strong under fast-fill conditions, and therefore, the jet may have caused the thermocouple to oscillate. As proof, because the

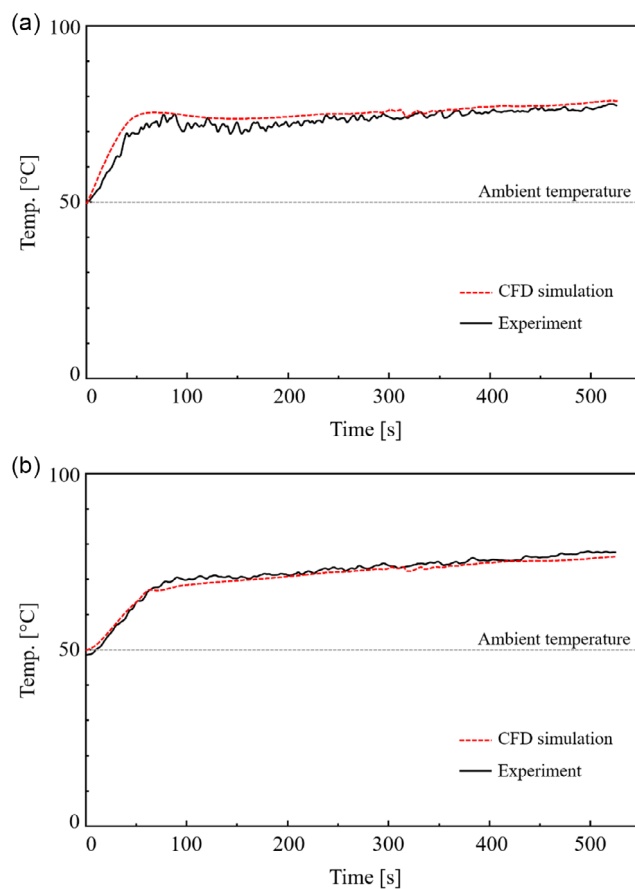


Figure 8. Validation of 244.0 L CFD tank model against corresponding experimental fueling data for the slow-fill condition. a) Hydrogen temperature, TC2. b) Liner surface temperature, TC3. The comparison was conducted under the following fueling conditions: an ambient temperature of 50.0 °C, an initial gas pressure of 5.2 MPa, and an APRR of 7.6 MPa min⁻¹.

thermocouple, TC1, was installed on upper surface of the liner, and it is hard to consider the mounted location of TC1 to be influenced by the jet.

The temperatures simulated and measured on the surface of the liner (TC3) matched with an error of less than 3.0 °C. The thermal mass of the plastic liner is much larger than that of the thermocouples, which means that the large thermocouples' time constant does not cause a significant error in the measurement of the liner surface temperature. This comparison also indicates that the discrepancy of the hydrogen temperatures simulated and measured at the early stage of the fueling process at TC2 results from the thermocouple's large time constant.

For the comparison of the slow-fill, the simulated hydrogen temperature agreed with the corresponding experimental data. In this case, there was no large discrepancy in the simulated and measured hydrogen temperatures at the early stage of the fill. This is because the slower the fueling speed is, the smaller the temperature change over time will be, which reduces the sensitivity of the temperature measurement to the thermal time constant of the thermocouple. For the comparison of the liner temperatures, the simulated temperature correlated with the measured data.

These comparisons of the fast- and slow-fill data reveal that this large tank model also makes it possible to precisely simulate the thermal and fluid fields regardless of the fueling speed, as well as to evaluate the temperature on the surface of the liner that is in contact with hydrogen.

5. Evaluation of Maximum Hydrogen and Liner Surface Temperatures in Each Tank Model

In Section 4, the reliability of the CFD tank models was validated against the corresponding experimental data. In this section, the simulation data obtained in Section 4 were analyzed: the maximum hydrogen temperature and the maximum temperature on the liner surface, as well as the thermal field in each tank model. Through this evaluation, this study assesses how quickly the liner temperature rise follows that of hydrogen and how close the liner temperatures is to its upper limit, 85.0 °C, when the tank models are filled under real-world fueling conditions.

Figure 9 shows the maximum hydrogen and liner surface temperatures simulated with the 36.0 L tank model, and **Figure 10** portrays the graphic results of the thermal fields at 25%, 50%, 75%, and 100% of the total fueling time. Figure 10d also includes the flow field around the injector. The black mark in each graphic represents the position of the maximum hydrogen temperature. Identically, the maximum hydrogen and liner surface temperatures and the thermal fields of the fast-filling simulation performed with the 244.0 L tank are shown in **Figure 11** and **12**, and the results of the slow-filling simulation performed with the same 244.0 L tank are shown in **Figure 13** and **14**.

Figure 9, 11, and 13 show that the maximum hydrogen temperature in each simulation surged at the early stage of the fueling process before 25% of the fill duration had elapsed. However, the change in those maximum temperatures over time was small, and the temperatures increased with a smaller rate of change until the ends of the fills. When the maximum hydrogen temperatures sharply increased at the early stage of the fueling process, as the thermal field results show, significant nonuniformities in the temperature distribution were observed. With the generation of significant temperature maldistribution, a

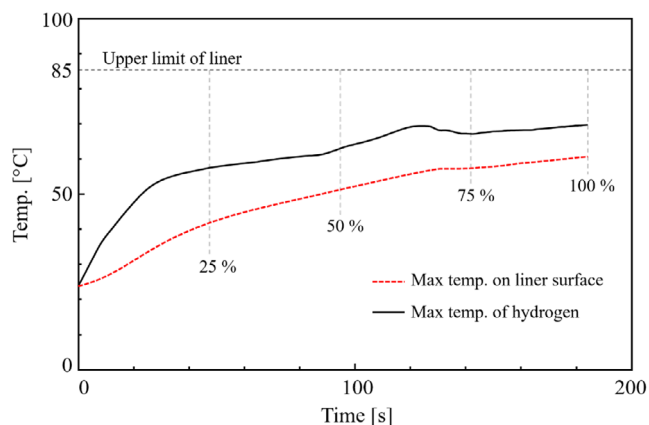


Figure 9. Maximum hydrogen and liner surface temperatures simulated with 36.0 L tank model.

high-temperature region was generated near the top and back liner surface of each tank model. As the maximum temperatures rate of change decreased over time, the high-temperature regions became more dispersed and the temperature maldistributions in the tanks gradually diminished. During this process, the maximum temperature position in each simulation moved toward the inlet side of the tank along the upper surface of the liner and then moved downward along the front surface of the liner. This is attributed to the flow field pattern generated along the front surface of the liner, as shown in Figure 10d. Heitsch et al.^[24] have also confirmed this flow pattern with their CFD tank model; thus, this study deduces that the flow pattern could commonly be generated when the thermal fields in FCEV tanks are in the process of becoming homogeneous. As mentioned before, the position of the maximum hydrogen temperature moves over time, but the highest temperatures throughout the fueling process were always found near the upper and back surfaces of the liners. This is because the buoyancy effect of hydrogen is strong; the gas heated of compression process is cooled by the inner liner surface and then the cooled hydrogen starts rising. Therefore, taking temperature measurements on the upper surfaces of the tank liners (oriented horizontally) would be practical, from a safety point of view, in real-world FCEV tanks.

The maximum temperatures on the inner liner surfaces did not increase as fast as those of the hydrogen gas as shown in Figure 9, 11, and 13. The liner temperatures were at least 7.0 °C lower than those of the hydrogen gas even though the high-temperature regions of gas were found near the liner surfaces, which suggests that the hydrogen's heat is not efficiently transferred to the inner liner surface in the form of convection. This may be due to low velocities along the liner surfaces that influence the convective heat transfer from hydrogen gas to the liners. The flow field in Figure 10d shows that the velocities along the front surface of the liner were extremely low in comparison with those at the injector outlet. This finding means that the convective heat transfer from the hydrogen to the liner was relatively small, and therefore, the liner surface temperature was not as high as that of the hydrogen gas. Melideo et al.^[25] demonstrated that injectors with upward angles are effective to reduce the thermal stratification caused by the incomplete mixing. Another similar study has also shown the effectiveness of upward injectors.^[26] This study infers that the upward injectors may have two benefits: one is to prevent the thermal fields in FCEV tanks from being unevenly distributed, and the other one is to increase the hydrogen's heat convective transfer coefficients to effectively transfer heat from the hydrogen gas to the liners.

The fueling conditions for each simulation detailed in Table 2 are based on the real-world fueling process defined by SAE J2601.^[17] Each result of the maximum liner temperature shows that there is a large temperature difference of at least 7.0 °C between the liner and hydrogen gas, and additionally the maximum liner temperatures were at least 12.0 °C lower than its upper limit temperature of 85.0 °C. After each fueling process concluded, the liner temperature would increase slightly because the hydrogen's heat continues to be transferred to the liner until equalization. However, the hydrogen temperature at the end of each fill did not reach 85.0 °C, so the liner temperature would not exceed that threshold. The SAE J2601 fueling protocol sets an

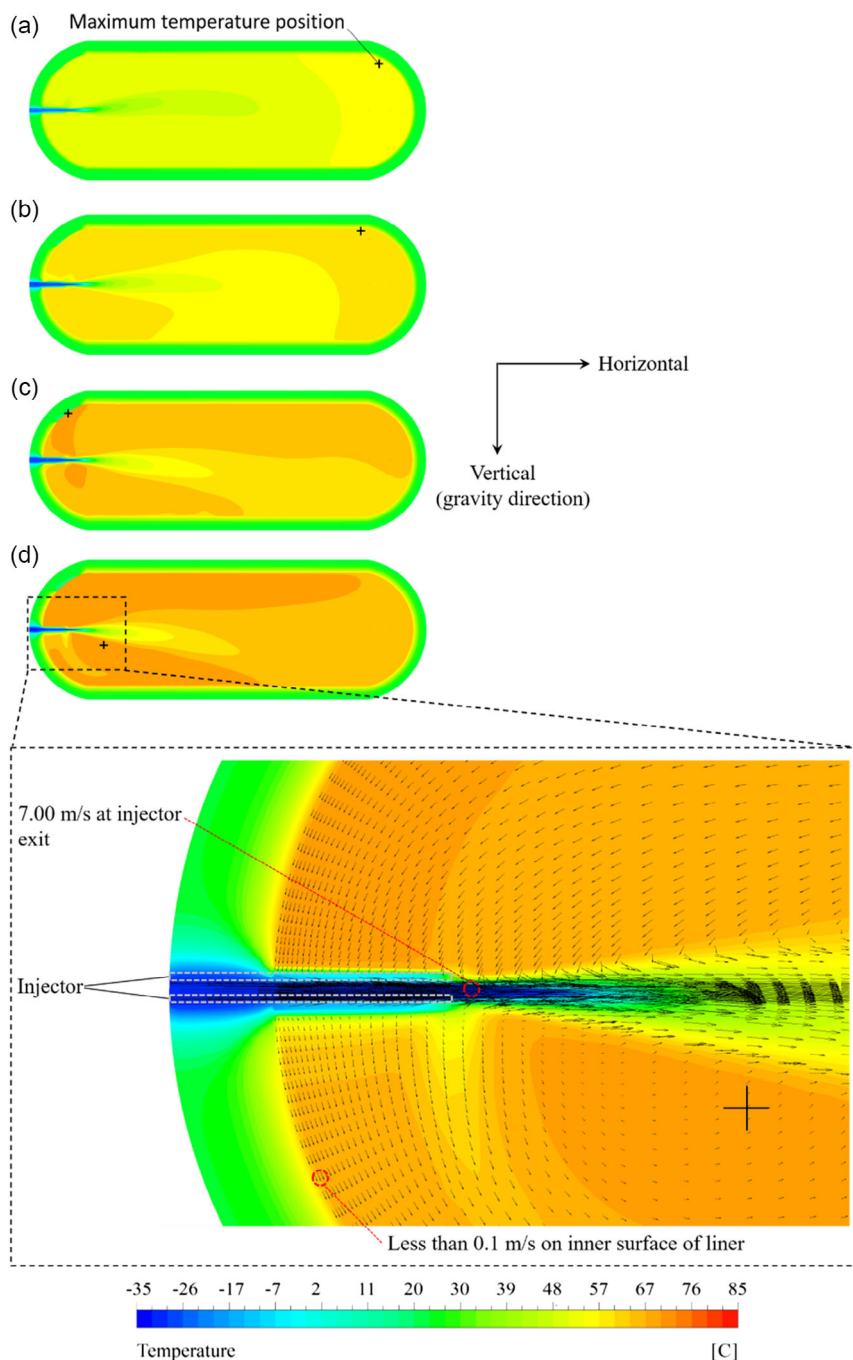


Figure 10. Thermal and flow fields inside 36.0 L tank during fast-fill simulation. a) 25% of total fueling time (46.5 s). b) 50% (93.0 s). c) 75% (140.0 s). d) 100% (186.0 s).

assumption where the initial hydrogen temperatures in FCEV tanks (prior to the fueling process) are higher than the ambient conditions (hot soak) due to being places in a parking garage or heated structure. This study did not include this assumption, and the initial hydrogen temperatures in the CFD simulations and experiments were identical to ambient conditions. If this assumption was taken into account, the difference between the maximum liner and the liner's upper limit temperatures,

12.0 K, would be much smaller. From this point, this study deduces that the fueling process set by SAE J2601 is sufficient to prevent the hydrogen temperatures in FCEV tanks from overheating within the ranges of the ambient temperature, precooling temperatures, and APRRs used in this study (Table 2). To ensure that the temperature of the liner remains below 85 °C for parameters outside of Table 2, further investigation may be required including wider ranges of ambient temperatures, precooling

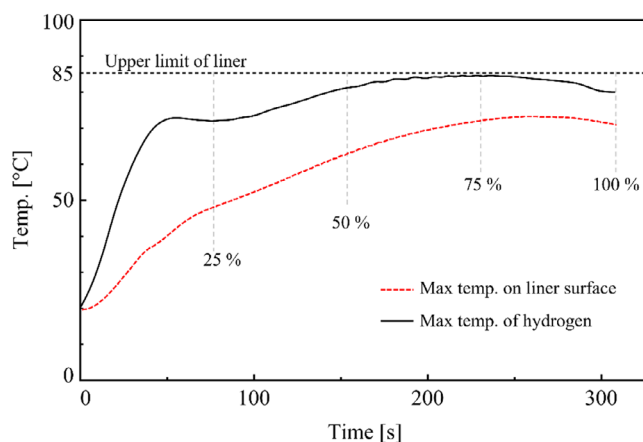


Figure 11. Maximum hydrogen and liner surface temperatures during fast-fill simulation of 244.0 L tank.

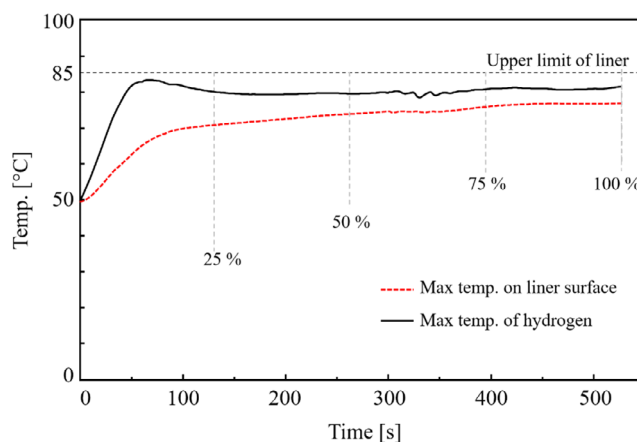


Figure 13. Maximum hydrogen and liner surface temperatures during slow-fill simulation of 244.0 L tank.

temperatures, APRRs, and tank sizes. The efforts may have the potential to improve the J2601 fueling protocol to fill up light-duty FCEVs more quickly, but as safely as now.

This study focuses only on the fueling process into light-duty FCEVs at retail stations. Currently, new hydrogen fueling technologies are being developed, and the market is expanding to include medium- and heavy-duty hydrogen-powered trucks

and residential fueling systems. With the development and expansion of these new technologies, further investigation will be required to confirm that fueling methodologies keep tank material temperatures within boundaries. This process will be crucial to ensure the safety of the new technologies and support the growth of the hydrogen into new markets. Also, the thermal fields in Figure 10, 12, and 14 show that the maximum gas

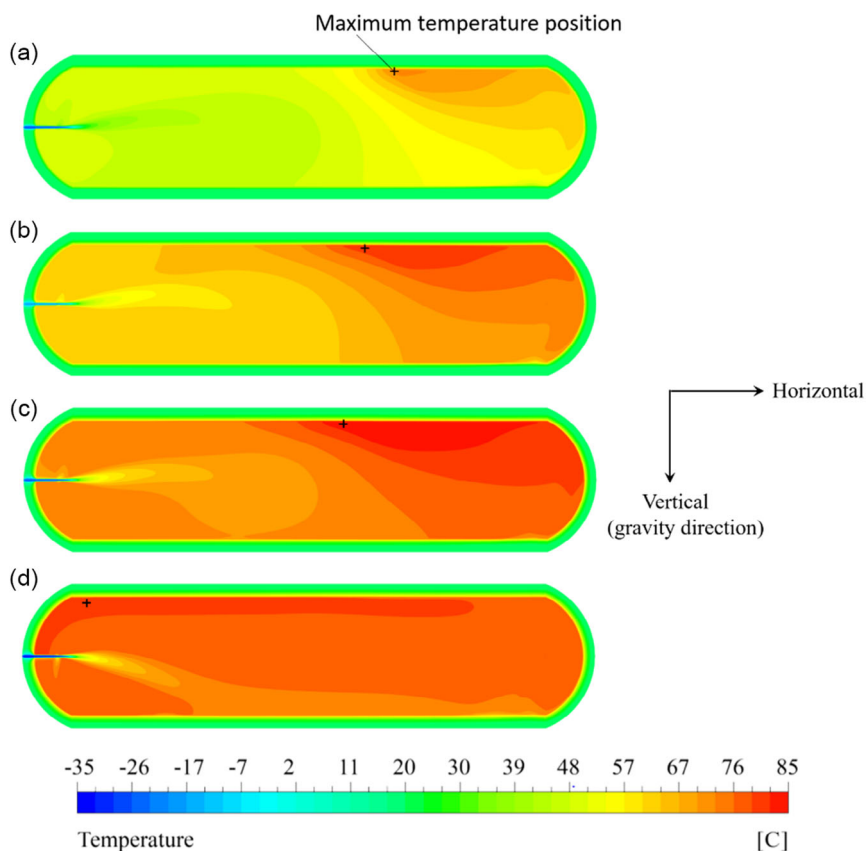


Figure 12. Thermal fields inside 244.0 L tank during fast-fill simulation. a) 25% of total fueling time (77.5 s). b) 50% (155.0 s). c) 75% (232.5 s). d) 100% (310.0 s).

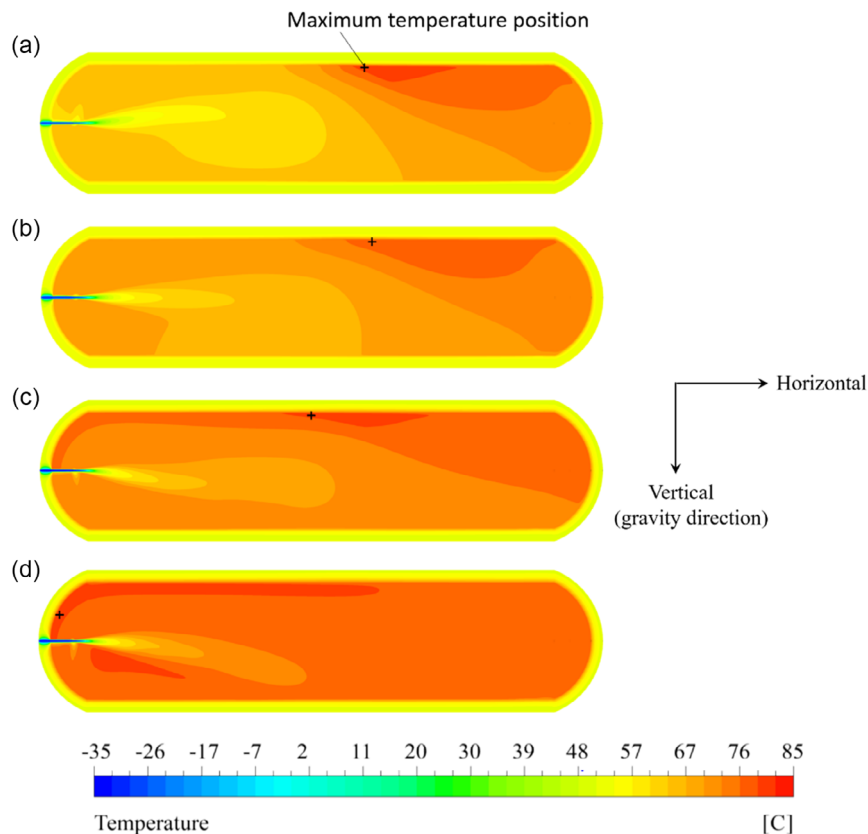


Figure 14. Thermal fields inside 244.0 L tank during slow-fill simulation. a) 25% of total fueling time. (134.0 s). b) 50% (268.0 s). c) 75% (402.0 s). d) 100% (536.0 s).

temperatures are always observed around the upper surface of the liner; however, the hydrogen temperature in a commercial FCEV tank is measured with a sensor mounted to the injector (on-tank valve),^[27] which means that the measured temperature may be significantly different to the maximum gas temperature in the tank. For this reason, this study suggests measuring the hydrogen temperature in FCEV tanks at locations adjacent to the upper surface of the liner, which would help keep a large amount of heat from being transferred from the high-temperature hydrogen to the neighboring liner.

6. Conclusion

This study explores CFD simulation results for two tank models (lower and upper limits of FCEV onboard storage system sizes outlined in SAE J2601) and whether the storage tank liners' remain at or below the upper temperature limit of 85.0 °C during the fueling process. These CFD tank models were initially validated with the corresponding experimental data. Through experimental validation, this study confirms discrepancies between the simulations and experiments, especially at the beginning of each fill, with the maximum discrepancy being 10 °C. This study infers that the discrepancies in each set of the simulations and experiments mainly result from the injector jet influencing the thermocouples; however, the simulation results overall agree

with the experimental data, so this study confirms the reliability of each tank model through the validation effort.

The maximum hydrogen and liner temperatures in each tank model are analyzed during the fueling process. At the early stage of the fueling process, significant maldistribution of the thermal fields is observed in the tank models, and the maximum temperature positions were found on the top and back surfaces of the liners. As the temperature maldistribution gradually disappears, each the position of the maximum temperature moves toward the inlet side of the tank along the upper surface of the liner. Although the maximum hydrogen temperature positions were found adjacent to the inner liner surfaces, the maximum temperatures on the liner surfaces were at least 7 °C lower than those of the hydrogen. Additionally, there was a significant difference of at least 12 °C discovered between the actual liner and liners' upper limit temperatures regardless of slow- or fast-fill conditions. In summary, within the range of parameters studied, the SAE J2601 fueling protocol will not cause a temperature increase above the threshold of the type IV tank liner material when the tanks are mounted horizontally and conditioned at or below ambient temperatures (non-hot soak condition). To quantitatively evaluate how safe the protocol is, further investigation will be required because the findings were obtained in a narrow range of fueling conditions. The efforts will lead to protocol improvements in filling FCEVs at faster rates than currently available.

Acknowledgements

This work was authored in part by the National Renewable Energy Laboratory, operated by Alliance for Sustainable Energy, LLC, for the U.S. Department of Energy (DOE) under Contract No. DE-AC36-08GO28308. Funding provided by the U.S. Department of Energy Office of Energy Efficiency and Renewable Energy Hydrogen and Fuel Cell Technologies Office. The authors acknowledge support from project partners Air Liquide, Honda, Shell, Toyota. The views expressed in the article do not necessarily represent the views of the DOE or the U.S. Government. This article has been contributed to by US Government contractors and their work is in the public domain in the USA.

Conflict of Interest

The authors declare no conflict of interest.

Data Availability Statement

Research data are not shared.

Keywords

computational fluid dynamics simulation, hydrogen fueling process, hydrogen temperature, plastic liner temperature, thermal and flow fields

Received: March 7, 2023

Revised: June 4, 2023

Published online: July 19, 2023

- [1] T. Kuroki, N. Sakoda, K. Shinzato, M. Monde, Y. Takata, *Int. J. Hydrogen Energy* **2018**, *43*, 2531.
- [2] L. Zhiyong, P. Xiangmin, M. Jianxin, *Int. J. Hydrogen Energy* **2011**, *36*, 4079.
- [3] B. C. Blazquez, *Int. J. Hydrogen Energy* **2019**, *44*, 495.
- [4] A. Elgowainy, K. Reddi, D. Y. Lee, N. Rustagi, E. Gupta, *Int. J. Hydrogen Energy* **2017**, *42*, 29067.
- [5] E. Kim, J. Park, J. Cho, I. Moon, *Int. J. Hydrogen Energy* **2013**, *38*, 1737.
- [6] M. Monde, M. Kosaka, *SAE Int. J. Altern. Powertrains* **2013**, *2*, 61.
- [7] S. C. Kim, S. H. Lee, K. B. Yoon, *Int. J. Hydrogen Energy* **2010**, *35*, 6830.
- [8] J. Xiao, X. Wang, P. Benard, R. Chahine, *Int. J. Hydrogen Energy* **2016**, *41*, 16316.
- [9] P. L. Woodfield, M. Monde, T. Takano, *J. Therm. Sci. Technol.* **2008**, *3*, 241.
- [10] C. N. Ranong, S. Maus, J. Hapke, G. Fieg, D. Wenger, *Heat Transfer Eng.* **2011**, *32*, 12.
- [11] T. Bourgeois, T. Brachmann, F. Barth, F. Ammouri, D. Baraldi, D. Melideo, B. Acosta-Iborra, D. Zaepffel, D. Saury, D. Lemonnier, *Int. J. Hydrogen Energy* **2017**, *42*, 13789.
- [12] V. Molkov, D. Dadashzadeh Makarov, *Int. J. Hydrogen Energy* **2019**, *44*, 4374.
- [13] T. Kuroki, N. Sakoda, K. Shinzato, M. Monde, Y. Takata, *Int. J. Hydrogen Energy* **2018**, *43*, 1846.
- [14] T. Kuroki, N. Sakoda, K. Shinzato, M. Monde, Y. Takata, *Int. J. Hydrogen Energy* **2018**, *43*, 5714.
- [15] C. J. B. Dicken, W. Merida, *J. Power Sources* **2007**, *165*, 324.
- [16] K. Yuan, H. Pan, Z. Liu, A. Andersson, *Processes* **2023**, *11*, 476.
- [17] SAE International Surface, Vehicle Standard. SAE Standard J2601, Revis. July **2014**.
- [18] S. J. Oh, J. H. Yoon, K. S. Jeon, J. Choi, *Int. J. Hydrogen Energy* **2022**, *47*, 25679.
- [19] J. Liu, H. Ma, S. Zheng, J. Zheng, Y. Zhao, *Int. J. Hydrogen Energy* **2021**, *46*, 20607.
- [20] D. Melideo, D. Baraldi, B. A. Iborra, R. O. Cebolla, P. Moretto, *Int. J. Hydrogen Energy* **2017**, *42*, 7304.
- [21] T. Johnson, R. Bozinoski, J. Ye, G. Startor, J. Zheng, J. Yang, *Int. J. Hydrogen Energy* **2015**, *40*, 9803.
- [22] Ansys Fluent, *Ansys Fluent R2019 Theory Guide* **2019**.
- [23] E. W. Lemmon, I. H. Bell, M. L. Huber, M. O. McLinden, *NIST Standard Reference Database 23: Reference Fluid Thermodynamic and Transport Properties-REFPROP, Version 10.0*, National Institute of Standards and Technology **2018**.
- [24] M. Heitsch, D. Baraldi, P. Moretto, *Int. J. Hydrogen Energy* **2011**, *36*, 2606.
- [25] D. Melideo, D. Baraldi, M. C. Galassi, N. D. M. Echevarria, B. A. Iborra, *Int. J. Hydrogen Energy* **2019**, *44*, 13569.
- [26] X. Wu, J. Liu, J. Shao, D. Guoming, *Int. J. Hydrogen Energy* **2021**, *46*, 29288.
- [27] Protocol for Heavy-Duty Hydrogen Refueling, https://lbtst.de/wp-content/uploads/2023/04/PRHYDE_Deliverable-D6-7_Results_as_Input_for_Standardisation_V1-2_final_Apr_2023.pdf
- [28] J. Schneider, G. Meadows, S. Mathison, M. Veenstra, J. Shim, R. Immel, M. Wistoft-Ibsen, S. Quong, M. Greisel, T. McGuire, P. Potzel, *SAE Int. J. Altern. Powertrains* **2014**, *3*, 257.